Journal of Biomolecular Techniques
10:163–176 © 1999 ABRF

METHODS & REVIEWS

Analytical Ultracentrifugation as a Contemporary Biomolecular Research Tool

James L. Cole[a] and Jeffrey C. Hansen[b]

[a]Department of Antiviral Research, Merck Research Laboratories, West Point, PA 19486, and [b]Department of Biochemistry, The University of Texas Health Science Center at San Antonio, San Antonio, TX 78284

Analytical ultracentrifugation has again become a widely used biomolecular research technique for determining sample purity, characterizing assembly and disassembly mechanisms of biomolecular complexes, determining subunit stoichiometries, detecting and characterizing macromolecular conformational changes, and measuring equilibrium constants and thermodynamic parameters for self- and hetero-associating systems. Concomitant with the availability of modern instrumentation is a strong need for biomedical scientists to become acquainted with the fundamental principles of analytical ultracentrifugation and the new data analysis methodologies that have greatly transformed this technique as it exists today. (J Biomol Tech 1999;10:163–176)

KEY WORDS: centrifugation, sedimentation velocity, sedimentation equilibrium, solution interactions, conformational changes.

ADDRESS CORRESPONDENCE AND REPRINT REQUESTS TO Jeffrey C. Hansen, Department of Biochemistry, The University of Texas Health Science Center at San Antonio, 7703 Floyd Curl Drive, San Antonio, TX 78284-7760 (email: hansen@bioc02.uthscsa.edu).

Analytical ultracentrifugation is an extremely versatile and powerful technique for characterizing the solution-state behavior of macromolecules. When coupled with contemporary data analysis methods, experiments performed in the analytical ultracentrifuge are capable of rigorously determining sample purity, characterizing assembly and disassembly mechanisms of biomolecular complexes, determining subunit stoichiometries, detecting and characterizing macromolecular conformational changes, and measuring equilibrium constants and thermodynamic parameters for self- and hetero-associating systems. After a lengthy hiatus, in which the instrumentation largely disappeared from laboratories throughout the world and the principles of analytical ultracentrifugation disappeared from classrooms,[1,2] a modern version of the analytical ultracentrifuge has again become available to the academic and industrial biomedical research communities. This review provides sufficient fundamental information about the new instrumentation and the corresponding developments in data analysis methods to allow readers of all levels to understand and appreciate the many experimental advantages offered by this reemergent biomolecular technique.

THE MODERN INSTRUMENT AND ITS EXPERIMENTAL USES

Analytical ultracentrifugation often is confused with more familiar types of procedures performed in preparative ultracentrifuges (eg, sucrose/glycerol gradient centrifugation, buoyant density centrifugation.) However, analytical ultracentrifuge experiments are fundamentally different in several key aspects. Most importantly, the sample is visualized in real time during sedimentation, allowing extremely accurate determination of hydrodynamic and thermodynamic parameters. In addition, the purpose of the experiment is to characterize key sample properties rather than

Novartis Exhibit 1006, Page 1 of 14

prepare or purify a sample for subsequent use. In contrast to many biophysical techniques, biomolecules are characterized during analytical ultracentrifugation in their native state under biologically relevant solution conditions. Because the experiments are performed in free solution, there are no complications caused by interactions with matrices or surfaces that can obscure interpretation of certain types of commonly used experiments, such as gel filtration.

Instrumentation

An analytical ultracentrifuge can be thought of as a marriage between a preparative ultracentrifuge and an optical detection system that is capable of directly measuring the sample concentration inside the centrifuge cell during sedimentation. The introduction of the Beckman Coulter XL-A analytical ultracentrifuge in 1992 is responsible for catalyzing renewed interest in this technique.[1–5,98] In contrast to the earlier version of this instrument (Model E), the XL-A is compact and easy to operate. The centrifugation parameters (eg, rotor speed, temperature) and data acquisition are under computer control, and experiments lasting from several hours to many days can be performed with minimal operator intervention. If desired, the data can be viewed or analyzed in real time as the experiment progresses.

The XL-A uses an absorbance optical system based on a xenon flashlamp and a scanning monochromator that allows measurement of sample concentration at wavelengths ranging from 200 to 800 nm.[6,7] Rayleigh interference optics subsequently were added to the XL-A, creating an analytical ultracentrifuge, the XL-I, that can simultaneously record data with both types of optical systems.[7–9] The Rayleigh interference optical system measures sample concentration based on refractive index changes. Each optical system has certain advantages and disadvantages.[7] Absorption optics are particularly sensitive for detection of macromolecules containing strong chromophores. For example, taking advantage of the intense amide absorption in the far ultraviolet (UV) and the strong lamp output at 230 nm, proteins can be characterized with good signal to noise ratio at concentrations as low as 10 μg/mL. Similarly, nucleic acids can be studied in the same concentration range by following their absorbance at 260 nm. For samples containing two or more components with different absorption spectra (ie, protein and nucleic acids), data can be obtained at multiple wavelengths during the same experiment to selectively monitor the several species in solution.[10,11]

The Rayleigh interference optical system is used to analyze macromolecules lacking intense chromophores (eg, polysaccharides) and samples that contain strongly absorbing buffer components (eg, ATP/GTP, $DTT_{oxidized}$). It also is the optical system of choice for characterizing very concentrated samples. The data from each cell are acquired simultaneously on a charge-couple device camera by the interference optical system, and the resulting rapid collection of large amounts of data is especially useful for certain types of sedimentation velocity experiments (discussed later). Interference optics are also useful for sedimentation equilibrium experiments that require a higher radial resolution than is provided by the absorbance optical system. Because the refractive index increment is fairly constant for most proteins, combining absorbance and interference data provides a method to determine protein extinction coefficients.[12]

In addition to the centrifuge, analytical ultracentrifuge experiments require specialized centrifuge cells and rotors. The centrifuge cells house the sample and reference buffer, and they are assembled before each experiment from a cell housing, quartz or sapphire windows, and one of several different types of centerpieces (Fig. 1). Rotors are available that hold three or seven cells together with a reference cell used for radial calibration purposes (4-hole and 8-hole rotors, respectively). Most sedimentation velocity experiments use a combination of a 4-hole rotor and centrifuge cells assembled with a double-sector centerpiece. This allows three different samples to be analyzed in each experiment. Equilibrium experiments are performed using 2-, 6-, or 8-sector cells.

Sample requirements are fairly modest, and preparation is straightforward. Depending on the application and optical system used, protein and nucleic acid concentrations ranging from 10 μg/mL to 5 mg/mL can be used. Required sample volumes are about 420 μL for sedimentation velocity experiments, 110 μL for standard 3-mm column sedimentation equilibrium experiments and 15 μL for "short-column" equilibrium experiments. For proteins, the ionic strength should be at least 50 mM to avoid nonideality caused by charge effects. Samples should be equilibrated with buffer using dialysis or gel filtration, and the equilibration buffer should be loaded into the reference sector (a common and potentially problematic mistake is to use reference buffer that is not identical to the sample-containing buffer). Disposable spin columns are quick and convenient for equilibrating small-sample volumes.

Experimental Applications: Sedimentation Velocity and Sedimentation Equilibrium

An analytical ultracentrifuge can be used to perform two types of experiments, referred to as sedimenta-

Novartis Exhibit 1006, Page 2 of 14

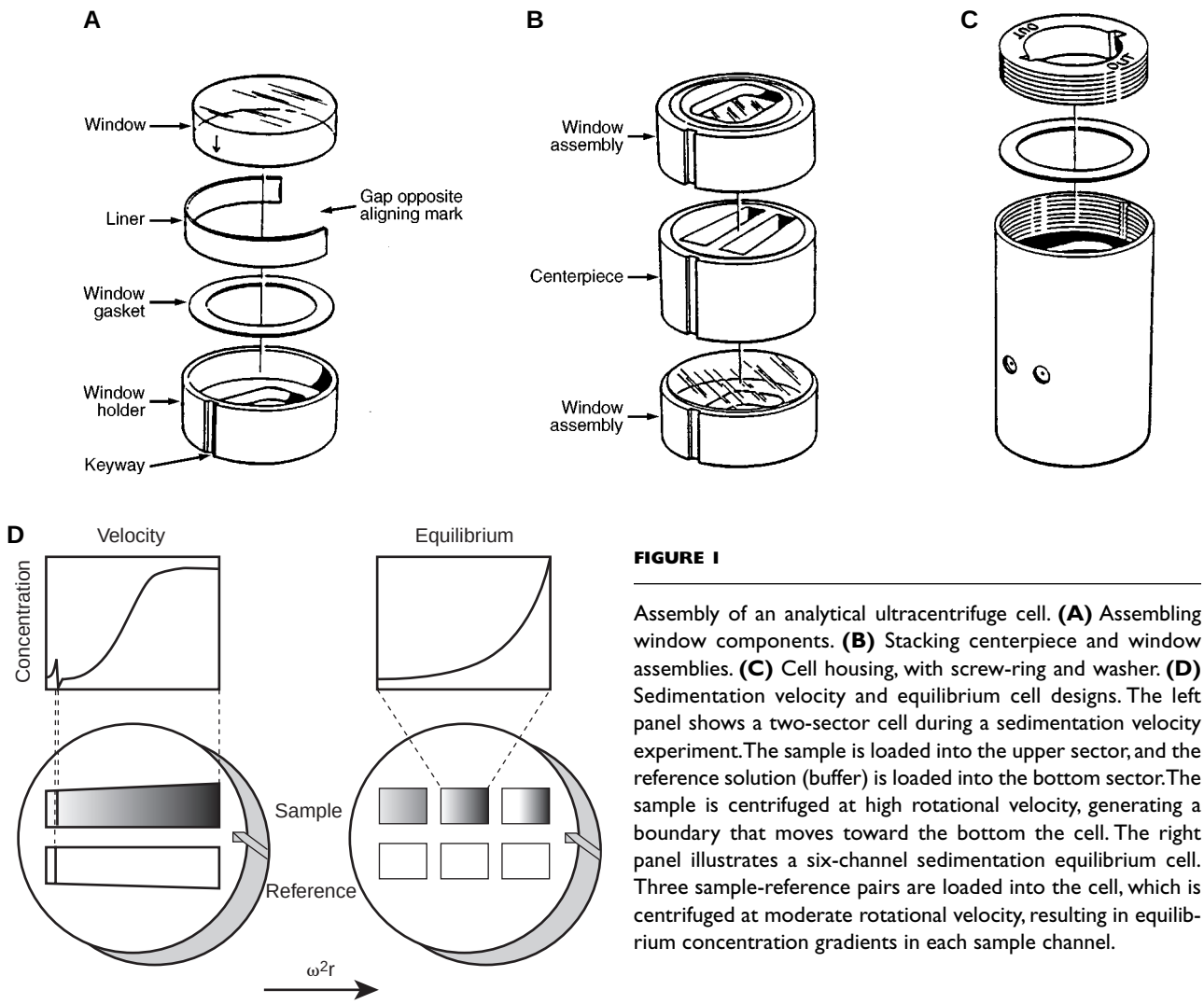

FIGURE 1

Assembly of an analytical ultracentrifuge cell. **(A)** Assembling window components. **(B)** Stacking centerpiece and window assemblies. **(C)** Cell housing, with screw-ring and washer. **(D)** Sedimentation velocity and equilibrium cell designs. The left panel shows a two-sector cell during a sedimentation velocity experiment. The sample is loaded into the upper sector, and the reference solution (buffer) is loaded into the bottom sector. The sample is centrifuged at high rotational velocity, generating a boundary that moves toward the bottom the cell. The right panel illustrates a six-channel sedimentation equilibrium cell. Three sample-reference pairs are loaded into the cell, which is centrifuged at moderate rotational velocity, resulting in equilibrium concentration gradients in each sample channel.

tion velocity and sedimentation equilibrium. Sedimentation velocity is a hydrodynamic technique and is sensitive to the mass and shape of the macromolecular species. In a sedimentation velocity experiment, a moving boundary is formed on application of a strong centrifugal field (Figs. 1*D* and 2). A series of scans (ie, measurements of sample concentration, c, as a function of radial distance, r) are recorded at regular intervals to determine the rate of movement and broadening of the boundary as a function of time. In contrast, sedimentation equilibrium is a thermodynamic technique that is sensitive to the mass but not the shape of the macromolecular species. These experiments are performed at lower speeds and measure the equilibrium concentration distribution of macromolecules that eventually forms when sedimentation is balanced by diffusion (Fig. 3). The sedimentation velocity and equilibrium measurements provide complementary information, and it is often useful to apply both techniques to a given problem.

Although the detailed mathematical theory that underlies sedimentation velocity and sedimentation equilibrium experiments can be complex,[13–18] many user-friendly data analysis programs allow a nonexpert to analyze analytical ultracentrifuge data with confidence (Table 1). Nevertheless, to obtain meaningful results and interpret them properly, it is necessary to be familiar with the fundamental principles.

In a sedimentation velocity experiment, application of a sufficiently large centrifugal force field leads to movement of solute molecules toward the bottom of the centrifuge cell. The rate of sedimentation in a centrifugal field, v, is described by the Svedberg equation:

$$s = v/\omega_2 r = M(1 - \bar{v}\rho)/Nf \qquad (1)$$

where s is the sedimentation coefficient, v is the velocity of the molecule, $\omega_2 r$ is the strength of the centrifugal field (ω is $2\pi \cdot rpm/60$ and r is the radial distance from the center of rotation), M is the molecular

Novartis Exhibit 1006, Page 3 of 14

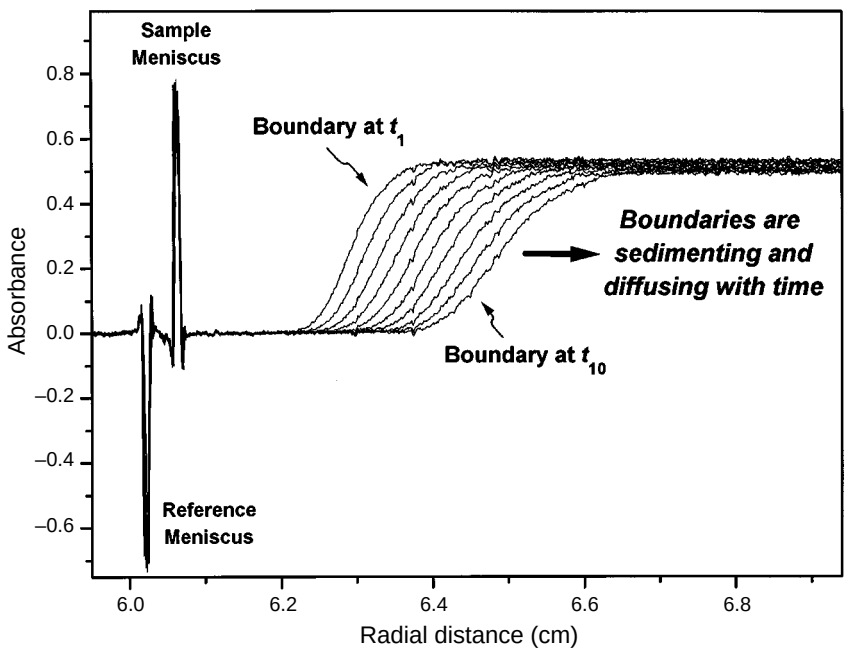

FIGURE 2

Sedimentation velocity data. A set of 10 scans were collected at about 9-minute intervals in a Beckman Coulter XL-I analytical ultracentrifuge using the absorbance optical system. The first and last scans are labeled t_1 and t_{10}, respectively. The first scan, collected after about 90 minutes of sedimentation, has already spread significantly because of diffusion.

mass, f is the frictional coefficient (which is directly related to macromolecular shape and size), ρ is the density of the solvent, N is Avogadro's number, and $\bar{\nu}$ is the partial specific volume of the solute. The solvent parameters (density and viscosity) are experimentally measurable or can be calculated from the solvent composition using tabulated data. For proteins, $\bar{\nu}$ in most cases can be calculated accurately from the amino acid composition. The program SEDNTERP (Table 1) implements these calculations.

Movement of the solute away from the air-solvent interface (ie, the meniscus) in a sedimentation velocity experiment leads to formation of a solute concentration gradient, called the boundary. Because it is a concentration gradient, the boundary sediments and diffuses with time, leading to "boundary spreading" over the course of the experiment (Fig. 2). The combination of sedimentation and diffusion in the ultracentrifuge cell is described in terms of the flow, J:

$$J = s\omega_2 rc - D(\partial c/\partial r) \qquad (2)$$

where s is the sedimentation coefficient as defined in equation 1, D is the diffusion coefficient, c is the solute concentration, and $\partial c/\partial r$ is the solute concentration gradient. From this theoretical overview, it can be seen that sedimentation velocity experiments can be used to determine s and D. Because D is directly proportional to f, sedimentation velocity also in some cases can provide M.

Figure 2 shows the scans obtained from a sedimentation velocity experiment performed in the XL-I analytical ultracentrifuge. Initially, the concentration of macromolecules is uniform throughout the centrifuge cell and $\partial c/\partial r = 0$. After a sufficient centrifugal force is applied, the boundary forms and subsequently moves toward the bottom of the cell at a rate proportional to the sedimentation coefficients of the components in the sample. The boundary spreading that occurs because of diffusion is evident as the experiment progresses (Fig. 2). The small decrease in concentration in the plateau region of successive scans is called radial dilution.[13,14,18] Various methods

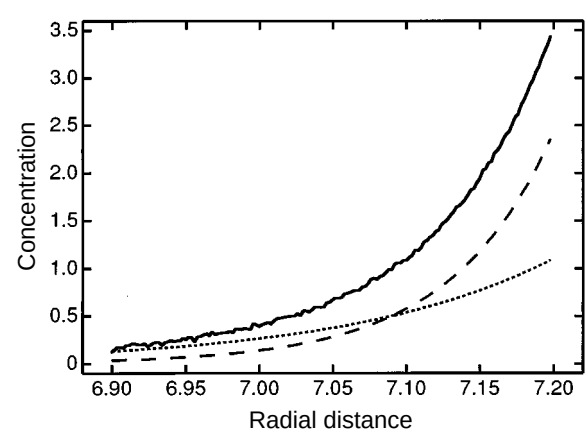

FIGURE 3

Sedimentation equilibrium data. Simulated data for a reversible monomer-dimer equilibrium: (—) total, (· · ·) monomer, (- - -) dimer. The concentration distribution of the dimer is steeper than that of the monomer, and the relative amounts of monomer and dimer at each radial point are determined by mass-action equilibrium.

Novartis Exhibit 1006, Page 4 of 14

TABLE 1

Software for Analysis of Sedimentation Data

Method	Application	Platform	Source[a]	Reference
Sedimentation Velocity				
Van-Holde-Weischet	UltraScan	UNIX, PC	1	22
Time derivative	DCDT, DCDT+, UltraScan, Beckman	PC, Macintosh, UNIX	1, 2, 3	25, 28
Direct fitting (approximate solution)	SVEDBERG[b]	PC	2, 4	32, 33
	LAMM	PC		34
Direct fitting (numerical solution)	UltraScan	UNIX, PC	1	35
	SEDFIT	PC	2	36
Second moment	UltraScan, Beckman	UNIX, PC	1, 3	
Hydrodynamic modeling	HYDRO	FORTRAN Source Code	5	48
	ATOB	PC	2	49
Sedimentation Equilibrium				
Nonlinear least squares	NONLIN	PC, Macintosh, VMS	2, 3	19
	UltraScan[c]	UNIX, PC	1	
	SEDEQ	PC	2	
Hetero-association	TWOCOMP	PC	2	43
Ω function	SEDProg	PC		39
General Utilities				
Graphics	XLAGRAPH	PC	2	
Parametric calculations	SEDNTERP, UltraScan	PC, UNIX	2	
Test for equilibrium	MATCH	PC	2	

[a]Sources: (1) http://biochem.uthscsa.edu/auc/software, (2) ftp://alpha.bbri.org/rasmb/ or or mirror site: http://www.cauma.uthscsa.edu/software, (3) Analysis software supplied with XL-A/XL-I, (4) http://www.jphilo.mailway.com, (5) http://leonardo.fcu.um.es/macromol/software.html.
[b]Public domain version 5.01 is available from source 2. A trial shareware version can be downloaded from source 4.
[c]Forthcoming.

for the analysis of sedimentation velocity boundaries are described in the following sections.

When the centrifugal force is sufficiently small, the process of diffusion significantly opposes the process of sedimentation, and an equilibrium concentration distribution of macromolecules eventually is obtained throughout the cell (Fig. 3). For an ideal noninteracting single component system (ie, simplest possible system to analyze), the equilibrium distribution obtained is an exponential function of the buoyant mass of the macromolecule, $M(1 - \bar{v}\rho)$, as described by Equation 3[15–17]:

$$c(r) = c_0 \exp[M(1 - \bar{v}\rho)\omega^2(r^2 - r_0^2)/2RT] \qquad (3)$$

where c(r) is the sample concentration at radial position r, c_0 is the sample concentration at a reference radial distance r_0, and R and T represent the gas constant and absolute temperature, respectively. Sedimentation equilibrium experiments provide an accurate way to determine M and consequently the oligomeric state of biomolecules, and they are not subject to complications from the matrix interactions, sample dilution, and assumption of globular shape that accompany determination of M by techniques such as gel filtration chromatography. Deviations from the simple exponential behavior described by Equation 3 can result from the presence in the sample of multiple noninteracting or interacting macromolecular species or thermodynamic nonideality. Equation 3 has been modified to account for these situations.[13,17,19,20] When various oligomeric species are in reversible equilibrium, the stoichiometries, equilibrium constants (K_{eq}) and even the thermodynamic parameters (ΔH, ΔS) that define the interactions can be obtained. Figure 3 shows an example of a reversible monomer-dimer equilibrium. In addition to the

Novartis Exhibit 1006, Page 5 of 14

TABLE 2

Problem-Solving Applications of the Analytical Ultracentrifuge

Experimental Application	Experiment Type	Analysis Methods	References
Biomolecular shape	SV	G(s)[a]	50, 51
		g(s*)[b]	52, 53
		Direct[c]	54–56
		Other[d]	57–60
Biomolecular conformational changes	SV	G(s)	50, 61–64
		g(s*)	65
		Other	57, 58, 66, 67
Assembly/disassembly of biomolecular complexes	SV	G(s)	68–71, 97
		g(s*)	53, 72–75
		Direct	76, 77
		Other	57, 78, 79
Molecular mass/subunit stoichiometry	SE	Direct[e]	52, 53, 71, 80–84
	SV	g(s*)	52, 53
		Direct	54, 56, 76, 77
Equilibrium constants for self-associating systems	SE	Direct	65, 84–90
		Ω function	91
	SV	g(s*)	86, 92, 93
Equilibrium constants for hetero-associating systems	SE	Direct	81, 83, 88, 94–96
		Ω function	47

SE, sedimentation equilibrium; SV, sedimentation velocity.
[a] van Holde and Weischet method.
[b]Time derivative (DCDT) method.
[c]Direct fitting to sedimentation velocity boundaries using approximate or numeric solutions to the Lamm equation.
[d]Other methods for determining sedimentation coefficients (eg, boundary midpoint, second moment.)
[e]Direct fitting of sedimentation equilibrium profiles using global nonlinear least-squares methods.

common application of characterizing oligomerization of a single component (self-association), sedimentation equilibrium is increasingly being used to analyze biologically interesting interactions between dissimilar partners (hetero-associations).

DATA ANALYSIS METHODS

In addition to the XL-A and XL-I instruments themselves, a major factor that has contributed to the renaissance of analytical ultracentrifugation is the concomitant availability of new and powerful methods for analysis of sedimentation velocity and equilibrium data. In this section, we describe these methods and their major applications. The methods are implemented in software that can be downloaded over the Internet (Table 1) or are included in the analysis package that comes with the XL-A and XL-I. The Reversible Associations in Structural and Molecular Biology (RASMB) group also maintains a list-server that facilitates effective and informative communication among researchers interested in analytical ultracentrifugation (network subscription: rasmb-manager@bbri.org).

Sedimentation Velocity Methods

The simplest method for analysis of sedimentation velocity experiments, which began in the days of manual analysis of the analog data produced by the Model E analytical ultracentrifuge, is to plot the natural logarithm of the radial position of the boundary midpoint or the second moment boundary position versus time.[5,13,15–18] The slope of this plot is proportional to $\omega^2 s$, in which s represents an apparent *average* sedimentation coefficient. Although it still is sometimes useful to perform single-point boundary analyses (Table 2), it generally is much more informative to analyze the *entire* boundary using one or more of three powerful methods that have been developed[3–5] (Table 2).

Novartis Exhibit 1006, Page 6 of 14

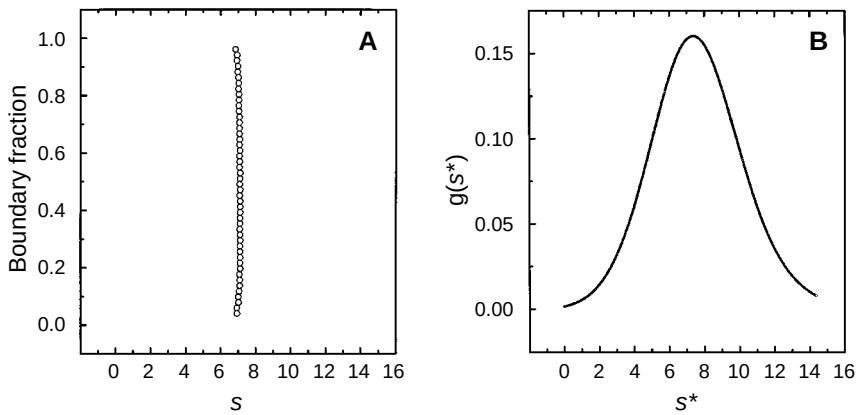

FIGURE 4

Analysis of a sedimentation a velocity experiment by the van Holde and Weischet **(A)** and time derivative **(B)** methods. Boundaries were simulated for an ideal oblate ellipsoid protein having a M = 100 kd, s = 7.1 S, D = 6.66 × 10^{-7}, and $\bar{\nu}$ = 0.74 using the UltraScan program. The simulated data were analyzed by the van Holde and Weischet[22] and time derivative methods[25] to obtain a G(s) plot **(A)** and g(s*) versus s* plot **(B)**.

The first of these methods was developed in 1978 by van Holde and Weischet to remove the contributions of diffusion to the shape of the boundaries,[22] because diffusional boundary spreading frequently hides the presence of heterogeneity in s because of multiple components in a sample. This method exploits the fact that transport due to sedimentation proceeds with the first power of time, whereas transport due to diffusion proceeds with the square root of time.[13–18,21] Consequently, by dividing the boundary of each scan into 20 to 50 equal divisions and extrapolating the apparent s calculated at each boundary division (which is an amalgam of sedimentation and diffusion) to infinite time, the actual s is obtained at each boundary division. These data are plotted as boundary fraction versus s_{actual} to obtain the integral distribution of s (Fig. 4*A*), abbreviated G(s). It has been demonstrated[23] that analysis of samples by this method over a 10- to 20-fold concentration range (which can be achieved by collecting data at multiple wavelengths) can indicate whether the sample consists of a single or multiple components (ie, is homogeneous or heterogeneous). In the case of heterogeneous samples, the method distinguishes whether the components are interacting or noninteracting, and if the latter, it quantifies the total number and amounts of each species present. The method also allows differentiating between components that are exhibiting ideal or nonideal behavior. The van Holde and Weischet method is useful for initially surveying unknown preparations by sedimentation velocity.[23] Because this method allows the investigator to identify and quantitate the presence of multiple species, it is particularly appropriate for analysis of the structure and stability of multicomponent biomolecular samples that are too complex to be analyzed by sedimentation equilibrium or other sedimentation velocity methods.[5,24]

A second useful velocity analysis technique is the time derivative (DCDT) method developed by Stafford.[25–28] This method converts the boundaries into an apparent differential distribution of s, g(s*) but does not remove the contributions of diffusion from the distribution profile. The g(s*) distributions are obtained by first subtracting pairs of scans to generate a set of $\Delta c/\Delta t$ data. The differences are then normalized and averaged to enhance the signal to noise ratio and subtract time-invariant baseline distortions.[25–28] The latter property makes it particularly useful for analyzing interference optical data. The improved signal to noise ratio, obtained by averaging a large number of scans collected over a short time, often allows the investigator to study very low concentrations of proteins (eg, 10 to 100 μg/mL). The results obtained by this method are plotted as g(s*) versus s* (Fig. 4*B*). This method can be used to study homogeneous samples and heterogeneous noninteracting and interacting systems provided that, in the latter cases, the multiple components separate sufficiently during sedimentation to form distinct peaks in the g(s*) versus s* plots. For single homogeneous species (including tightly associated complexes), the g(s*) plot can be fit to a gaussian distribution to determine M; the standard deviation of the distribution (σ) is proportional to D, and s/D is directly proportional to M.[29] However, a good gaussian fit to the g(s*) versus s* distribution in and of itself is not a rigorous diagnostic for sample homogeneity, because the s* distribution is influenced by diffusion. Consequently, one of the other two types of sedimentation velocity methods must be used to demonstrate sample homogeneity. In the case of interacting systems, a concentration-dependent increase in the weight average sedimentation coefficient ($s_{20,W}$) obtained from the time derivative or G(s) methods is a definitive indication of mass action-driven association. Plots of g(s*) versus s* as a function of protein or ligand concentration often reveal the mechanism of self association.

The third method for analysis of velocity data involves direct fitting of the boundaries using approximate or numeric solutions to the Lamm equation.

Novartis Exhibit 1006, Page 7 of 14

The Lamm equation is the partial differential equation that describes transport of solutes in the sector-shaped cells used in sedimentation velocity experiments.[21] Methods based on approximate solutions include early versions by Holladay[30,31] and later the SVEDBERG program by Philo[32,33] and LAMM program by Behlke and Ristau.[34] Methods based on numeric solutions have been developed by Demeler and Saber[35] and by Schuck.[36] These approaches are model dependent; the fitting process is based on equations that describe specific models such as a single ideal component or monomer-dimer associating system. In principle, they can provide a rigorous diagnostic for sample homogeneity. When used under the appropriate conditions, model-dependent fitting methods directly determine s and D, and consequently, M and f can accurately be calculated provided $\bar{v}$ is known. Each of these methods have specific strengths in terms of how they should be applied experimentally, and the original papers should be consulted for these details (Table 1).

Sedimentation Equilibrium Methods

Methods for analysis of sedimentation equilibrium data can be divided into model-independent and model-dependent approaches. Graphical model-independent data analysis methods date from the time of the Model E centrifuge, before the advent of digital data collection and fast computers capable of global nonlinear least squares fitting. Model-independent methods are most useful at the initial stages of sample analysis, when the goal is to survey sample behavior, or for comparative analysis of samples that are too complex to be fit directly by model-dependent methods. In contrast, model-dependent analysis involve direct fitting of the sedimentation equilibrium concentration gradients to mathematical functions describing various physical models, such as single ideal species, a monomer $\rightarrow$ n-mer self-associating system, or an A + B $\rightarrow$ C hetero-associating system. Direct fitting is the method of choice for detailed quantitative analysis of sedimentation equilibrium data. This approach provides the best-fit values and the associated statistical uncertainties in the fitting parameters (eg, molecular mass, oligomer stoichiometry, association constants) and a statistical basis to discriminate among alternative physical models.[37,38]

The simplest model-independent approach is to plot ln c versus r^2.[13,14,17] According to Equation 3, the slope of this line is directly proportional to M. Although linearity of this plot has been taken as evidence that a sample contains a single ideal species, this method can be insensitive to heterogeneity, particularly if the concentration gradient is shallow. Moreover, $d(\ln c)/dr^2$ can be calculated on a point-by-point basis to create a plot of the apparent weight-average molecular weight ($M_{w,app}$) versus c. For a sample containing a ideal single component, $M_{w,app}$ is a constant as a function of c. An increase in $M_{w,app}$ with c indicates mass action–driven association. In this case, it is useful to overlay on the same plot data obtained from several samples over a range of loading concentrations, rotor speeds, or both. For a reversibly self-associating system, all of the data lie on a smooth curve, whereas a noninteracting or slowly equilibrating system gives rise to family of nonsuperimposing curves. Differentiation increases the intrinsic noise in the raw data. An alternative approach that avoids differentiation is to calculate the omega function (ω), which also is a smooth, continuous function of the total concentration c and can be used to obtain $M_{w,app}$.[39]

When analyzing a sample by analytical ultracentrifugation for the first time, it is strongly recommended to use both sedimentation velocity and sedimentation equilibrium approaches to survey the behavior of the biomolecule over a broad range of sample concentrations, rotor speeds, or other experimental conditions. In the case of sedimentation equilibrium, the short-column method[40,41] is ideal for this purpose. Because it requires little material (~15 μL), many samples can be analyzed simultaneously (eg, 28 in the 8-hole rotor), and equilibrium is achieved rapidly (~16-fold faster than with the standard 3-mm column, 110-μL samples.) Centerpieces that hold four 15-μL samples (700- to 800-μm column height) have been designed specifically for short-column experiments.[41] The average molecular weight in each channel is determined using a model-independent method or nonlinear least squares fitting. Data obtained over a range of loading concentrations and rotor speeds are then used to assess whether the sample is homogeneous, mass action–driven self-association is occurring, or thermodynamic nonideality is significant.[42] When combined with the complementary information obtained from sedimentation velocity experiments, the investigator can simultaneously delineate the fundamental solution-state behavior of the macromolecule being studied and facilitate subsequent characterization of the sample by the model-dependent sedimentation equilibrium approaches.

More sophisticated data analysis methods are required to characterize self- and hetero-associating systems. In these cases, global methods should be employed in which multiple datasets that are collected over a wide range of sample loading concentrations and rotor speeds are simultaneously fit to a specific model for the association phenomenon using nonlinear least squares algorithms. The global fitting approach helps to ensure that a unique solution is

Novartis Exhibit 1006, Page 8 of 14

obtained and greatly reduces the statistical uncertainty in the parameters.[37,38] Global fitting of sedimentation equilibrium data is implemented in the NONLIN[19] program (Tables 1 and 2). Other global analysis software is available (Table 1), and global fitting methods also can be programmed by the user within several general-purpose data analysis packages (eg, IGOR, SigmaPlot, Origin, MLAB).

Although it is more difficult to reliably fit data for hetero-associating systems, a number of methods have been developed for this purpose.[11,43,44] For hetero-associating systems, sedimentation equilibrium data obtained using interference optics or absorption optics at only one wavelength contain contributions from both components (ie, A and B). Frequently, these data are insufficient to produce a well-defined and unique minimum in the fit error surface, even when using global fitting procedures. It therefore is necessary to introduce additional constraints into the fitting algorithm. One such approach is to resolve the contributions of A and B to the overall equilibrium concentration gradients. When the components have different absorption spectra (eg, proteins and nucleic acids), the investigator can globally fit absorbance data collected at multiple wavelengths to obtain the individual concentration gradients of A and B.[10,11] Alternatively, sedimentation equilibrium can be performed using a preparative ultracentrifuge.[45] The tubes are fractionated after the run using a specially designed device,[46] and the individual components are detected and quantitated using gel electrophoresis or radioactive or fluorescent tags. The resulting equilibrium concentration gradients are analyzed in the same way as those obtained in the analytical ultracentrifuge. If the components cannot be resolved, additional constraints to the global fitting algorithm involving the conservation of mass or signal should be applied.[43,44] Methods that use the ω function also can be used to characterize self- and hetero-associating systems by global model-dependent fitting.[39,47,91]

PROBLEM-SOLVING USING THE ANALYTICAL ULTRACENTRIFUGE

The previous sections describe the fundamental principles and recent advances required for the nonexpert to grasp how analytical ultracentrifugation can be used to address contemporary research problems. As little as a few years ago, it was possible to illustrate the specific uses of analytical ultracentrifugation by reviewing selected papers chosen from the relatively small body of literature available.[5] However, during the past 5 years, more than 500 papers have been published in which the XL-A or XL-I has been used, and it no longer is possible or appropriate to attempt to document the broad and varied problem-solving capabilities of the analytical ultracentrifuge by focusing on a limited number of examples. Instead, users at all levels of expertise must become familiar with the rapidly expanding body of analytical ultracentrifuge literature. Table 2 provides references to a wide variety of papers about experiments that have used the analytical ultracentrifuge in conjunction with one or more of the digital analysis methods described earlier to address the varied types of problems for which analytical ultracentrifugation is best suited. For many of these reports, we subsequently discuss the scientific context in which analytical ultracentrifugation was used. Taken together, this information allows the interested researcher to immediately embrace analytical ultracentrifugation and rapidly proceed toward using this remarkable technique to its fullest.

Sedimentation Velocity

Biomolecular Shape

Rogers et al.[51] used the G(*s*) profiles and the sedimentation coefficients derived from them to determine the effect of N-terminal deletion mutations on the shape of the lipid-free forms of human apolipoprotein A-I (apo hA-I). In addition to showing that native apo hA-I is highly elongated, the sedimentation studies defined two specific regions within the N-terminus whose deletion led to significant changes in hydrodynamic shape. This structural information subsequently was correlated with functional effects of the N-terminal deletions on lipid binding and lecithin-cholesterol acyltransferase activation by apo hA-I. Fleming et al.[52] used the sedimentation coefficients obtained from g(*s**) distributions to characterize the hexameric structure of the *N*-ethylmaleimide-sensitive fusion (NSF) protein involved in intracellular trafficking. These studies, together with complementary information derived from electron microscopy and light scattering, provided novel information on the mechanism of action of NSF and related ATPases. Rich et al.[56] used direct finite element fitting of sedimentation velocity boundaries to derive the *s* and D used for determination of the solution shape of the *Staphylococcus aureus* collagen adhesin. Wagschal et al.[59] used second moment sedimentation coefficients to derive the hydrodynamic shape of a trimeric coiled-coil–forming model peptide and showed that the oxidized and reduced forms of the trimer have different conformations. They further showed that the different shapes of the oxidized and reduced forms of the peptide trimer were in excellent agreement with those expected from the x-ray structures of related coiled-coil complexes.

Novartis Exhibit 1006, Page 9 of 14

It should be noted that when *s* and M are known accurately, calculation of hydrodynamic shape parameters (eg, frictional ratio, axial ratio) has been automated by programs such as SEDINTERP and UltraScan (Table 1).

Biomolecular Conformational Changes

Tse et al.[63] used the G(*s*) method to demonstrate that acetylation of the core histone N termini was a potent inducer of chromatin unfolding (indicated by a large decrease in *s* without a change in M) and that acetylation-induced unfolding was correlated with a 15-fold increase in transcriptional activity of the chromatin template. Kar et al.[65] used the g(*s**) method to show that a Zn^{2+}-dependent conformation change in the cyanobacterial SmtB repressor protein prevented the repressor from binding to DNA, abolishing the ability of SmtB to inhibit transcription of SmtB-dependent genes. Fletcher et al.[66] used the average sedimentation coefficient derived from G(*s*) plots and the average effective radius obtained from agarose gel electrophoresis to determine how histone octamer density influences salt-dependent chromatin folding. These studies demonstrated that the minimum unit required for chromatin folding is a run of two to three nucleosomes and showed for the first time that quantitative analysis of agarose gel electrophoresis data yields the same information as the average sedimentation coefficient.

Assembly and Disassembly of Biomolecular Complexes

Beernink and Morrical[97] used the G(*s*) method to characterize the stability of oligomers of the bacteriophage T4 uvsY recombination protein. These experiments demonstrated that uvsY self-assembles into single-stranded DNA–binding hexamers, which then associate further into higher oligomers. Moreover, oligomerization of uvsY hexamer was shown to depend strongly on the salt concentration. These sedimentation results provided novel insight into the structure and function of the uvsY protein.

Behal et al.[68] provided a elegant demonstration of the utility of the G(*s*) method for characterizing very large biomolecular complexes by determining for the first time the assembly pathway for the 3 million dalton 30S E2 subunit of pyruvate dehydrogenase from its monomeric constituents. The g(*s**) method was used by Rippe et al.[53] to demonstrate that the *Escherichia coli* transcription activator protein NtrC is a dimer (by deriving *s* and D and calculating M). They went on to use the g(*s**) method to characterize association of the NtrC dimer with two different DNA binding sites. The g(*s**) method also was employed effectively by Toedt et al.[74] to demonstrate that the assembly kinetics of tobacco mosaic virus depended on whether native or mutant coat proteins were used for the reconstitution reactions.

Direct fitting of sedimentation velocity boundaries using the program SVEDBERG (Table 1) allowed Fujita et al.[76] to determine the pH dependence of human erythrocyte spectrin disassembly, which helped provide insight into the structure-function relationships that control assembly of physiologically relevant spectrin oligomers. Schwarz et al.[79] used the second moment sedimentation coefficient to demonstrate cooperative oligomerization of defined oligonucleosome model systems; in this case, the "monomer" consisted of an assemblage of 96 histone proteins and approximately 2.5 kb of DNA and had an M of 3×10^6 daltons, whereas the oligomers sedimented between several hundred and several thousand S. The in vitro oligomerization process was shown to absolutely depend on the core histone N termini and was postulated to be functionally related to the long-range fiber-fiber interactions found in interphase chromosomes.

Molecular Mass and Subunit Stoichiometry

In addition to determination of biomolecular shape, Fleming et al.[52] and Rippke et al.[53] used the g(*s**) method to ascertain subunit stoichiometry from the experimentally determined M. Direct fitting methods also have been used effectively to calculate M and hence stoichiometry. For example, Leroux et al.,[77] using the SVEDBERG program to determine the stoichiometry of small heat shock proteins (smHSP), showed that oligomerization of smHSPs is a prerequisite for binding unfolded polypeptides and subsequent chaperone activity. Similarly, the work of Rosenfeld et al.[54] used the SVEDBERG method to show that the recombinant form of the human agouti-related protein involved in the control of feeding is monomeric at physiologic concentrations.

Equilibrium Constants for Self-Associating Systems

Although this area traditionally has involved application of sedimentation equilibrium approaches, the time derivative sedimentation velocity method also can be used to obtain K_{eq} when used appropriately. The laboratory of Correia has been the clear leader in this area, with the group publishing numerous important papers during the past several years in which g(*s**) data have been used to calculate the energetics of drug-induced tubulin self-association.[92,93] The

Novartis Exhibit 1006, Page 10 of 14

quantitative sedimentation velocity work from the Correia group has made many critical contributions to understanding the basic and clinical aspects of tubulin function, and these papers are classics that should be read by all practicing centrifugationists.

A theme that connects each of the papers outlined in the sedimentation velocity section and those described later in the sedimentation equilibrium section is that analytical ultracentrifugation invariably was used in conjunction with other techniques to best answer the biologic questions being asked.

Sedimentation Equilibrium

Molecular Mass and Subunit Stoichiometry

Several research groups have employed sedimentation equilibrium methods to characterize subunit stoichiometries in protein-protein and protein-nucleic acid complexes. In addition to the sedimentation velocity work described earlier, Rippe et al.[53] used sedimentation equilibrium methods to demonstrate that NtrC exists as a dimer and to characterize the stoichiometry of the protein-DNA complexes. In the unphosphorylated state, one NtrC dimer binds noncooperatively to each binding site in a DNA oligonucleotide containing the enhancer sequence (two NtrC binding sites). In contrast, the phosphorylated protein cooperatively formed an octameric complex at the enhancer sequence. Tennyson et al.[82] demonstrated that *Saccharomyces cerevisiae* DNA topoisomerase II exists as a stable dimer in solution; however, the K_d was too low to be measured by this technique. The sedimentation results were confirmed using subunit exchange assays, which demonstrated that the dimer is also kinetically stable.

Wu et al.[83] demonstrated that the cAMP response element–binding protein (CREB) is a monomer in solution. The stoichiometry of CREB binding to DNA was defined by labeling a cAMP response element DNA with fluorescein and monitoring the sedimentation experiments at 494 nm to selectively observe the DNA component. It was found that CREB cooperatively assembles on DNA to form dimers.

Equilibrium Constants for Self-Associating System

Several researchers used equilibrium analytical ultracentrifugation to define equilibrium constants for self-associating systems. Kar et al.[65] found that the self-association of the cynanobacterial repressor SmtB fit best to a monomer-dimer-tetramer equilibrium, with dimer as the predominant species under their conditions. Binding of Zn^{2+} increased the strength of the monomer-dimer association about 100-fold, but the dimer-tetramer equilibrium was unaffected. Abril et al.[90] characterized self-association of the phage ϕ29 p6 protein over a wide range of protein, temperature, and salt concentrations. At low concentrations, a monomer-dimer equilibrium is operative, but at the high physiologic protein concentration of 1 mM, further association occurs, and a monomer-hexamer or an indefinite isodesmic model is compatible with the data. Parker et al.[89] observed that phage P22 scaffolding protein reversibly self-associated Global fits to sedimentation equilibrium with NONLIN were compatible with several different models: monomer-dimer-n-mer (n = 4 to 6). A two-species plot indicated that the most reasonable model is monomer-dimer-tetramer.

Equilibrium Constants for Hetero-associating Systems

Several groups measured the affinity of heteromeric protein-protein interactions using sedimentation equilibrium. Shi et al.[94] defined the interaction of a soluble lectin domain of the IgE receptor, sCD23, with an IgE fragment. The sedimentation equilibria indicated that IgE has two, low-affinity binding sites for CD23, with K_d of about 10^{-5} M. Temperature-dependent measurements demonstrated that the two binding events have different thermodynamics, suggesting two distinct binding modes.

Darawashe et al.[95] characterized dissociation of the *Salmonella typhimurium* tryptophan synthase $alpha_2$-$beta_2$ complex by guanidine isothiocyanate using a model in which the two alpha subunits sequentially dissociate from a stable $beta_2$ subunit. Measurements of the two equilibrium constants as a function of guanidine concentration effectively excluded strong cooperativity in the dissociation reaction.

Cole et al.[96] characterized dimerization of human ribonuclease L on binding of 2'- to 5'-linked adenosine oligomers. Multiwavelength sedimentation equilibrium data were consistent with a model in which a single activator binds to the monomeric enzyme and subsequently induces dimerization. Fluorescent anisotropy measurements confirmed this model and gave equilibrium constants close to those determined by sedimentation.

ACKNOWLEDGMENTS

We are grateful to Dr. B. Demeler for providing constructive comments and V. Schirf for performing the data simulation and analyses shown in Figure 4. This work was supported by NIH grant GM45916 and NSF grant DBI9724273 to J.C. Hansen.

Novartis Exhibit 1006, Page 11 of 14

REFERENCES

1. Schachman HK. Is there a future for the ultracentrifuge? In Harding SE, Rowe AJ, Horton JC (ed): *Analytical Ultracentrifugation in Biochemistry and Polymer Science,* Cambridge, UK: Royal Society of Chemistry, 1992:3–15.
2. van Holde KE, Hansen JC. Analytical ultracentrifugation from 1924 to the present: a remarkable history. *Chemtracts Biochem Mol Biol* 1998;11:933–943.
3. Schuster TM, Toedt JM. New revolutions in the evolution of analytical ultracentrifugation. *Curr Opin Struct Biol* 1996;6:650–658.
4. Hensley P. Defining the structure and stability of macromolecular assemblies in solution: the re-emergence of analytical ultracentrifugation as a practical tool. *Structure* 1996;4:367–373.
5. Hansen JC, Lebowitz J, Demeler B. Analytical ultracentrifugation of complex macromolecular systems. *Biochemistry* 1994;33:13155–13163.
6. Giebeler R. The optima XL-A: a new analytical ultracentrifuge with a novel precision absorption optical system. In Harding SE, Rowe AJ, Horton JC (ed): *Analytical Ultracentrifugation in Biochemistry and Polymer Science.* Cambridge, UK Royal Society of Chemistry, 1992:16–25.
7. Laue TM. *Choosing Which Optical System of the Optima XL-I Analytical Centrifuge to Use.* Beckman Coulter Application Information, number A-1821-A,1996 (URL: http://www.beckman.com/Beckman/biorsrch/prodinfo/xla/a_1821a.asp).
8. Furst A. The XL-I analytical ultracentrifuge with Rayleigh interference optics. *Eur J Biochem* 1997;35:307–310.
9. Yphantis DA, Lary JW, Stafford WF, et al. On-line data acquisition for the Rayleigh interference optical system of the analytical ultracentrifuge. In Shuster TM, Laue TM (ed): *Modern Analytical Ultracentrifugation.* Boston: Birkhauser, 1994:209–226.
10. Lewis MS, Shrager RI, Kim S-J. Analysis of protein-nucleic acid and protein-protein interactions using multi-wavelength scans from the XL-A analytical centrifuge. In Shuster TM, Laue TM (eds): *Modern Analytical Ultracentrifugation,* Boston: Birkhauser, 1994: 94–115.
11. Howlett GJ. Analysis of hetero-associating systems by sedimentation equilibrium. *Chemtracts Biochem Mol Biol* 1998;11:950–959.
12. Gray RA, Stern A, Bewley T, Shire SJ. *Rapid Determination of Spectrophotometric Absorptivity by Analytical Ultracentrifugation.* Beckman Coulter Application Information, number A-1815-A, 1995 (URL: http://www.beckman.com/beckman/biorsrch/prodinfo/xla/pdf/a_1815a.pdf).
13. Cantor CR, Schimmel PR. *Biophysical Chemistry,* part II. San Francisco: WH Freeman, 1980.
14. Ralston G. *Introduction to Analytical Ultracentrifugation.* Fullerton, CA: Beckman Instruments, 1993.
15. Schachman HK. *Ultracentrifugation in Biochemistry.* New York: Academic Press, 1959.
16. Tanford C. *Physical Chemistry of Macromolecules.* New York: John Wiley and Sons, 1961.
17. van Holde KE. Sedimentation analysis of proteins. In Neurath H, Hill RH (ed): *The Proteins,* I. New York: Academic Press, 1975:225–291.
18. van Holde KE. *Physical Biochemistry,* 2nd ed. Englewood Cliffs, NJ: Prentice-Hall, 1985.
19. Johnson ML, Correia JJ, Yphantis DA, Halvorson HR. Analysis of data from the analytical ultracentrifuge by nonlinear least squares techniques. *Biophys J* 1981;36: 575–588.
20. McRorie DK, Voelker PJ. *Self-Associating Systems in the Analytical Ultracentrifuge.* Fullerton, CA: Beckman Instruments, 1993.
21. Fujita H. *Foundations of Ultracentrifugal Analysis.* New York: Wiley, 1975.
22. van Holde KE, Weischet WO. Boundary analysis of sedimentation-velocity experiments with monodisperse and paucidisperse solutes. *Biopolymers* 1978;17:1387–1403.
23. Demeler B, Saber H, Hansen JC. Identification and interpretation of complexity in sedimentation velocity boundaries. *Biophys J* 1997;72:397–407.
24. Carruthers LC, Schirf V, Demeler B, Hansen JC. Sedimentation velocity analysis of macromolecular assemblies. *Methods Enzymol* 1999 (in press).
25. Stafford WF. Boundary analysis in sedimentation transport experiments: a procedure for obtaining sedimentation coefficient distributions using the time derivative of the concentration profile. *Anal Biochem* 1992;203: 295–301.
26. Stafford WF. Methods for obtaining sedimentation coefficient distributions. In Harding SE, Rowe AJ, Horton JC (ed): *Analytical Ultracentrifugation in Biochemistry and Polymer Science.* Cambridge, UK: Royal Society of Chemistry, 1992:359–393.
27. Stafford WF. Sedimentation boundary analysis of interacting systems: use of the apparent sedimentation coefficient distribution function. In Shuster TM, Laue TM (ed): *Modern Analytical Ultracentrifugation.* Boston: Birkhauser, 1994:119–137.
28. Stafford WF. Boundary analysis in sedimentation velocity experiments. *Methods Enzymol* 1994;240:478–501.
29. Stafford WF. Sedimentation velocity spins a new weave for an old fabric. *Curr Opin Biotechnol* 1997;8:14–24.
30. Holladay LA. Simultaneous rapid estimation of sedimentation coefficient and molecular weight. *Biophys Chem* 1980;303–308.
31. Holladay LA. An approximate solution to the Lamm equation. *Biophys Chem* 1979;10:187–190.
32. Philo JS. Measuring sedimentation, diffusion, and molecular weights of small molecules by direct fitting of sedimentation velocity concentration profiles. In Shuster TM, Laue TM (ed): *Modern Analytical Ultracentrifugation.* Boston: Birkhauser, 1994:156–170.
33. Philo JS. An improved function for fitting sedimentation velocity data for low-molecular-weight solutes. *Biophys J* 1997;72:435–44.
34. Behlke J, Ristau O. Molecular mass determination by sedimentation velocity experiments and direct fitting of the concentration profiles. *Biophys J* 1997;72:428–434.
35. Demeler B, Saber H. Determination of molecular parameters by fitting sedimentation data to finite-element solutions of the Lamm equation. *Biophys J* 1998;74: 444–454.
36. Schuck P. Sedimentation analysis of noninteracting and self-associating solutes using numerical solutions to the Lamm equation. *Biophys J* 1998;75:1503–1512.
37. Johnson ML, Straume M. Comments on the analysis of sedimentation equilibrium experiments In Shuster TM, Laue TM (ed): *Modern Analytical Ultracentrifugation.* Boston: Birkhauser, 1994:37–65.
38. Johnson ML, Faunt LM. Parameter estimation by least-squares methods. *Methods Enzymol* 1992;210:1–37.

Novartis Exhibit 1006, Page 12 of 14

39. Milthorpe BK, Jeffrey PD, Nichol LW. The direct analysis of sedimentation equilibrium results obtained with polymerising systems. *Biophys Chem* 1975;3:169–176.
40. van Holde KE, Baldwin RL. Rapid attainment of sedimentation equilibrium. *J Phys Chem* 1958;62:734–743.
41. Yphantis DA. Rapid determination of molecular weights of proteins and peptides. *Ann NY Acad Sci* 1960;88: 586–601.
42. Laue TM. *Short Column Sedimentation Equilibrium Analysis for Rapid Characterization of Macromolecules in Solution*. Beckman Coulter Application Information DS-835, 1992 (URL: http://www.beckman.com/Beckman/articles/ds835/ds835.asp).
43. Minton AP. Alternative strategies for the characterization of associations in muticomponent solutions via measurements of sedimentation equilibrium. *Prog Colloid Polymer Sci* 1997;107:11–19.
44. Philo JS. Improving sedimentation equilibrium analysis of mixed associations using numerical constraints to impose mass or signal conservation. *Methods Enzymol* 1999 (in press).
45. Minton AP. Analytical centrifugation with preparative ultracentrifuges. *Biophys Biochem* 1989;176:209–216.
46. Darawshe S, Rivas G, Minton AP. Rapid and accurate microfractionation of the contents of small centrifuge tubes: application in the measurement of molecular weight of proteins via sedimentation equilibrium. *Biophys Biochem* 1993;209:130–135.
47. Winzor DJ, Jacobsen MP, Wills PR. Direct analysis of sedimentation equilibrium distributions reflecting complex formation between dissimilar reactants. *Biochemistry* 1998;37:2226–2233.
48. Garcia de la Torre J, Navarro S, Lopez Martinez MC, Diaz FG, Lopez Cascales JJ. HYDRO: a computer program for the prediction of hydrodynamic properties of macromolecules. *Biophys J* 1994;67:530–531.
49. Byron O. Construction of hydrodynamic bead models from high-resolution x-ray crystallographic or nuclear magnetic resonance data. *Biophys J* 1997;72:408–415.
50. Carruthers LM, Bednar J, Woodcock CL, Hansen JC. Linker histones stabilize the intrinsic salt-dependent folding of nucleosomal arrays: mechanistic ramifications for higher-order chromatin folding. *Biochemistry* 1998;37:14776–14787.
51. Rogers DP, Roberts LM, Lebowitz J, et al. The lipid-free structure of apolipoprotein A-I: effects of amino-terminal deletions. *Biochemistry* 1998;37:11714–11725.
52. Fleming KG, Hohl TM, Yu RC, et al. A revised model for the oligomeric state of the *N*-ethylmaleimide-sensitive fusion protein, NSF. *J Biol Chem* 1998;273: 15675–15681.
53. Rippe K, Mucke N, Schulz A. Association states of the transcription activator protein NtrC from *E. coli* determined by analytical ultracentrifugation. *J Mol Biol* 1998; 278:915–933.
54. Rosenfeld RD, Zeni L, Welcher AA, et al. Biochemical, biophysical, and pharmacological characterization of bacterially expressed human agouti-related protein. *Biochemistry* 1998;37:16041–15052.
55. Zubrzycki IZ, Frankel LK, Russo PS, Bricker TM. Hydrodynamic studies on the manganese-stabilizing protein of photosystem II. *Biochemistry* 1998;37:13553–13558.
56. Rich RL, Demeler B, Ashby K, et al. Domain structure of the *Staphylococcus aureus* collagen adhesin. *Biochemistry* 1998;37:15423–15433.
57. Tse C, Fletcher TM, Hansen JC. Enhanced transcription factor access to arrays of histone H3/H4 tetramer-DNA complexes in vitro: implications for replication and transcription. *Proc Natl Acad Sci USA* 1998;95:12169–12173.
58. Fless GM, Kirk EW, Klezovitch O, et al. Effect of phospholipase A2 digestion on the conformation and lysine/fibrinogen binding properties of human lipoprotein[a]. *J Lipid Res* 1999;40:583–592.
59. Wagschal K, Tripet B, Hodges RS. De novo design of a model peptide sequence to examine the effects of single amino acid substitutions in the hydrophobic core on both stability and oligomerization state of coiled-coils. *J Mol Biol* 1999;285:785–803.
60. Gutierrez MM, Tsai SW, Phillips ML, et al. Studying low-density lipoprotein-monoclonal antibody complexes using dynamic laser light scattering and analytical ultracentrifugation. *Biochemistry* 1999;38:1284–1292.
61. Tse C, Hansen JC. Hybrid trypsinized nucleosomal arrays: identification of multiple functional roles of the H2A/H2B and H3/H4 N-termini in chromatin fiber compaction. *Biochemistry* 1997;36:11381–11388.
62. Bullard JM, Demeler B, Spremulli LL. Expression and characterization of a human mitochondrial phenylalanyl-tRNA synthetase. *Biochemistry* 1999;38:2716–2724.
63. Tse C, Sera T, Wolffe AP, Hansen JC. Acetylation-induced decondensation of nucleosomal arrays dramatically facilitates transcription by RNA polymerase III. *Mol Cell Biol* 1998;18:4629–4638.
64. Logie C, Tse C, Hansen JC, Peterson CL. The core histone N-terminal domains are required for multiple rounds of catalytic chromatin remodeling by the SWI/SNF and RSC complexes. *Biochemistry* 1999;38: 2514–2522.
65. Kar SR, Adams AC, Lebowitz J, Taylor KB, Hall LM. The cyanobacterial repressor SmtB is predominantly a dimer and binds two Zn^{2+} ions per subunit. *Biochemistry* 1997;36:15343–15348.
66. Fletcher TM, Serwer P, Hansen JC. Quantitative analysis of macromolecular conformational changes using agarose gel electrophoresis: application to chromatin folding. *Biochemistry* 1994;33:10859–10863.
67. Fletcher TM, Hansen JC. Core histone tail domains mediate oligonucleosome folding and nucleosomal DNA organization through distinct molecular mechanisms. *J Biol Chem* 1995;270:25359–25362.
68. Behal RH, DeBuysere MS, Demeler B, Hansen JC, Olson MS. Pyruvate dehydrogenase multienzyme complex. Characterization of assembly intermediates by sedimentation velocity analysis. *J Biol Chem* 1994;269: 31372–31377.
69. Mendoza JA, Demeler B, Horowitz PM. Alteration of the quaternary structure of cpn60 modulates chaperonin-assisted folding: implications for the mechanism of chaperonin action. *J Biol Chem* 1994;269:2447–2451.
70. Musatov A, Robinson NC. Detergent-solubilized monomeric and dimeric cytochrome bc1 isolated from bovine heart. *Biochemistry* 1994;33:13005–130012.
71. Anant JS, Desnoyers L, Machius M, et al. Mechanism of Rab geranylgeranylation: formation of the catalytic ternary complex. *Biochemistry* 1998;37:12559–12568.
72. Liu J, Laue TM, Choi HU, Tang LH, Rosenberg L. The self-association of biglycan from bovine articular cartilage. *J Biol Chem* 1994;269:28366–28373.

Novartis Exhibit 1006, Page 13 of 14

73. McLachlin DT, Bestard JA, Dunn SD. The beta and delta subunits of the *Escherichia coli* ATP synthase interact via residues in their C-terminal regions. *J Biol Chem* 1998;273:15162–15168.
74. Toedt JM, Braswell EH, Schuster TM, et al. Biophysical characterization of a designed TMV coat protein mutant, R46G, that elicits a moderate hypersensitivity response in *Nicotiana sylvestris*. *Protein Sci* 1999;8:261–270.
75. Hsu YR, Nybo R, Sullivan JK, et al. Heparin is essential for a single keratinocyte growth factor molecule to bind and form a complex with two molecules of the extracellular domain of its receptor. *Biochemistry* 1999; 38:2523–2534.
76. Fujita T, Ralston GB, Morris MB. Biophysical properties of human erythrocyte spectrin at alkaline pH: implications for spectrin structure, function, and association. *Biochemistry* 1998;37:264–271.
77. Leroux MR, Melki R, Gordon B, Batelier G, Candido EP. Structure-function studies on small heat shock protein oligomeric assembly and interaction with unfolded polypeptides. *J Biol Chem* 1997;272:24646–24656.
78. Fletcher TM, Krishnan U, Serwer P, Hansen JC. Quantitative agarose gel electrophoresis of chromatin: nucleosome-dependent changes in charge, sharp, and deformability at low ionic strength. *Biochemistry* 1994;33:2226–2233.
79. Schwarz PM, Felthauser A, Fletcher TM, Hansen JC. Reversible oligonucleosome self-association: dependence on divalent cations and core histone tail domains. *Biochemistry* 1996;35:4009–4015.
80. Syto R, Murgolo NJ, Braswell EH, et al. Structural and biological stability of the human interleukin 10 homodimer. *Biochemistry* 1998;37:16943–16951.
81. Saez C, Thielens NM, Bjes ES, Esser AF. Association of terminal complement proteins in solution and modulation by suramin. *Biochemistry* 1999;38:6807–6816.
82. Tennyson RB, Lindsley JE. Type II DNA topoisomerase from *Saccharomyces cerevisiae* is a stable dimer. *Biochemistry* 1997;36:6107–6114.
83. Wu X, Spiro C, Owen WG, McMurray CT. cAMP response element-binding protein monomers cooperatively assemble to form dimers on DNA. *J Biol Chem* 1998;273:20820–20827.
84. Zhong M, Kim SJ, Wu C. Sensitivity of Drosophila heat shock transcription factor to low pH. *J Biol Chem* 1999; 274:3135–3140.
85. Daugherty MA, Brenowitz M, Fried MG. The TATA-binding protein from *Saccharomyces cerevisiae* oligomerizes in solution at micromolar concentrations to form tetramers and octamers. *J Mol Biol* 1999;285: 1389–1399.
86. Cole JL. Characterization of human cytomegalovirus protease dimerization by analytical centrifugation. *Biochemistry* 1996;35:15601–15610.
87. Steinmetzer K, Behlke J, Brantl S. Plasmid pIP501 encoded transcriptional repressor CopR binds to its target DNA as a dimer. *J Mol Biol* 1998;283:595–603.
88. Rusinova E, Ross JBA, Laue TM, Sowers LC, Senear DF. Linkage between operator binding and dimer to octamer self-assembly of bacteriophage lambda cI repressor. *Biochemistry* 1997;36:12994–3003.
89. Parker MH, Stafford WF 3rd, Prevelige PE Jr. Bacteriophage P22 scaffolding protein forms oligomers in solution. *J Mol Biol* 1997;268:655–665.
90. Abril AM, Salas M, Andreu JM, Hermoso JM, Rivas G. Phage ϕ29 protein p6 is in a monomer-dimer equilibrium that shifts to higher association states at the millimolar concentrations found *in vivo*. *Biochemistry* 1997; 36:11901–11908.
91. Begg GE, Morris MB, Ralston GB. Comparison of the salt-dependent self-association of brain and erythroid spectrin. *Biochemistry* 1997;36:6977–6985.
92. Vulevic B, Lobert S, Correia JJ. Role of guanine nucleotides in the vinblastine-induced self-association of tubulin: effects of guanosine α,β-methylenetriphosphate and guanosine α,β-methylenediphosphate. *Biochemistry* 1997;36:12828–12835.
93. Lobert S, Ingram JW, Hill BT, Correia JJ. A comparison of thermodynamic parameters for vinorelbine- and vinflunine-induced tubulin self-association by sedimentation velocity. *Mol Pharmacol* 1998;53:908–915.
94. Shi J, Ghirlando R, Beavil RL, et al. Interaction of the low-affinity receptor CD23/Fc epsilonRII lectin domain with the Fc epsilon3–4 fragment of human immunoglobulin E. *Biochemistry* 1997;36:2112–2122.
95. Darawshe S, Millar DB, Ahmed SA, Miles EW, Minton AP. Dissociation equilibria of the tryptophan synthase alpha 2 beta 2 complex in saline buffer and guanidine isothiocyanate, as studied by sedimentation equilibrium. *Biophys Chem* 1997;69:53–62.
96. Cole JL, Carroll SS, Blue ES, Viscount T, Kuo LC. Activation of RNase L by 2',5'-oligoadenylates. Biophysical characterization. *J Biol Chem* 1997;272:19187–19192.
97. Beernink HT, Morrical SW. The uvsY recombination protein of bacteriophage T4 forms hexamers in the presence and absence of single-stranded DNA. *Biochemistry* 1998;37:5673–5681.
98. Laue TM, Stafford WF. Modern applications of the analytical ultracentrifuge. *Annu Rev Biophys Biomol Struct* 1999;28:75–100.

Novartis Exhibit 1006, Page 14 of 14